SUPPLEMENTARY INFORMATION

Tension directly stabilizes reconstituted kinetochore-microtubule attachments

Bungo Akiyoshi, Krishna K. Sarangapani, Andrew F. Powers, Christian R. Nelson, Steve L. Reichow, Hugo Arellano-Santoyo, Tamir Gonen, Jeffrey A. Ranish, Charles L. Asbury and Sue Biggins

1. Supplementary Figures and Legends

2. Supplementary Notes

3. Supplementary Tables

Table S1. Dsn1-FLAG mass spectrometry list (excel file link).

Table S2. Parameters for exponential curve fits shown in Fig. 4c and 4d.

Table S3. Yeast strains used in this study.

Table S4. Plasmids used in this study.

4. Supplementary Movie legends

Movie S1. Cse4-GFP kinetochore particles track with depolymerizing microtubule tips.

Movie S2. Nuf2-3GFP kinetochore particles track with shortening tips.

Movie S3. Purified kinetochore particles couple force to dynamic microtubules.

5. Supplementary References

1. Supplementary figures and legends

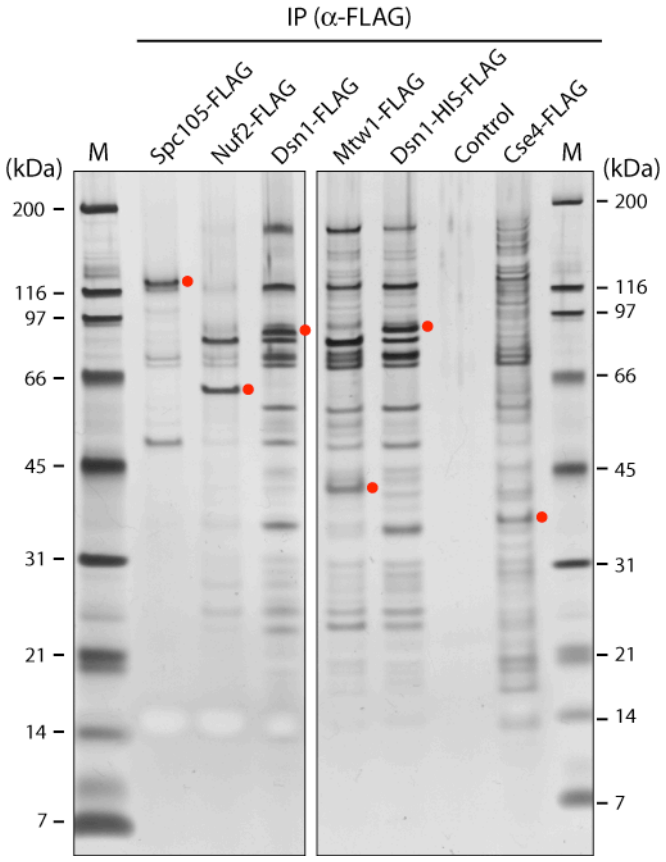

Figure S1. Affinity-purification of various kinetochore subcomplexes.

The indicated FLAG-tagged kinetochore proteins (FLAG: 4 kDa) were purified using anti-FLAG antibodies, eluted with FLAG peptide and analyzed by SDS-PAGE followed by silver-staining. An untagged strain was used as a control. Purification of Mis12 kinetochore subcomplex components (Mtw1, Dsn1) isolates most core kinetochore proteins while purifications of the Spc105, Nuf2, and Cse4 proteins under similar conditions do not. Red circles indicate epitope-tagged proteins.

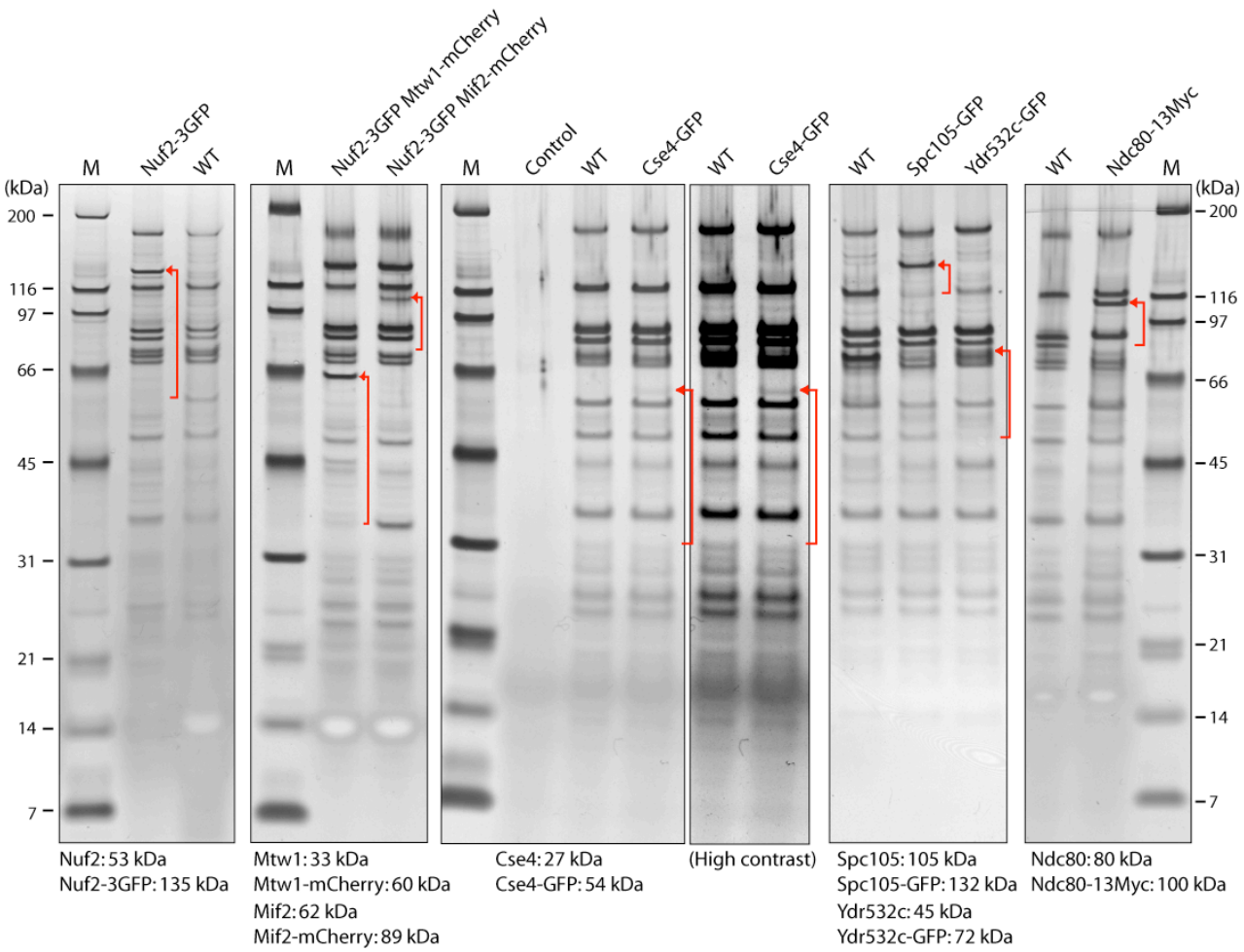

Figure S2. Determination of the composition of purified kinetochore particles.

Kinetochore particles were purified using Dsn1-FLAG from strains expressing the indicated fusion proteins. Band shifts (disappearance and appearance of bands marked by red arrows) by predicted molecular weights (1GFP: 27 kDa, 3GFP: 82 kDa, mCherry: 27 kDa, 13Myc: 20 kDa) identify the tagged proteins. KMN (KNL1/Spc105, Mis12, Ndc80 subcomplexes) components are the most abundant proteins in the sample, while Cse4, Mif2 and components of the ten-subunit Dam1 complex (not shown) appear to be present in substoichiometric ratios to KMN.

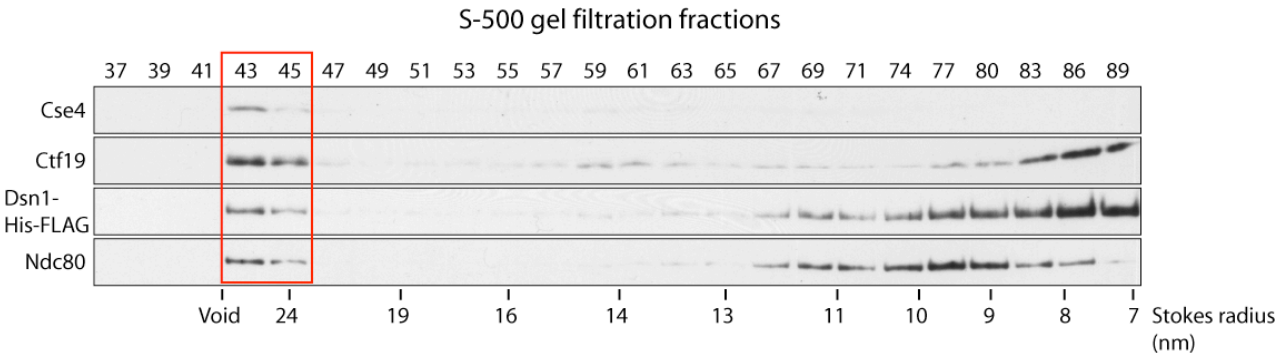

Figure S3. Analysis of S-500 gel filtration fractions over a wide range.

Purified Dsn1-His-FLAG samples were analyzed by immunoblotting against the indicated kinetochore proteins after S-500 size exclusion chromatography (fraction numbers indicated above blots). Note that the reported Stokes radius for the Ndc80 subcomplex is ~9 nm, Mis12 complex ~7 nm, COMA ~6 nm[1,2]. The wide distribution of kinetochore proteins could reflect multiple species within the cell and/or deterioration of complexes prior to, or during, the chromatography.

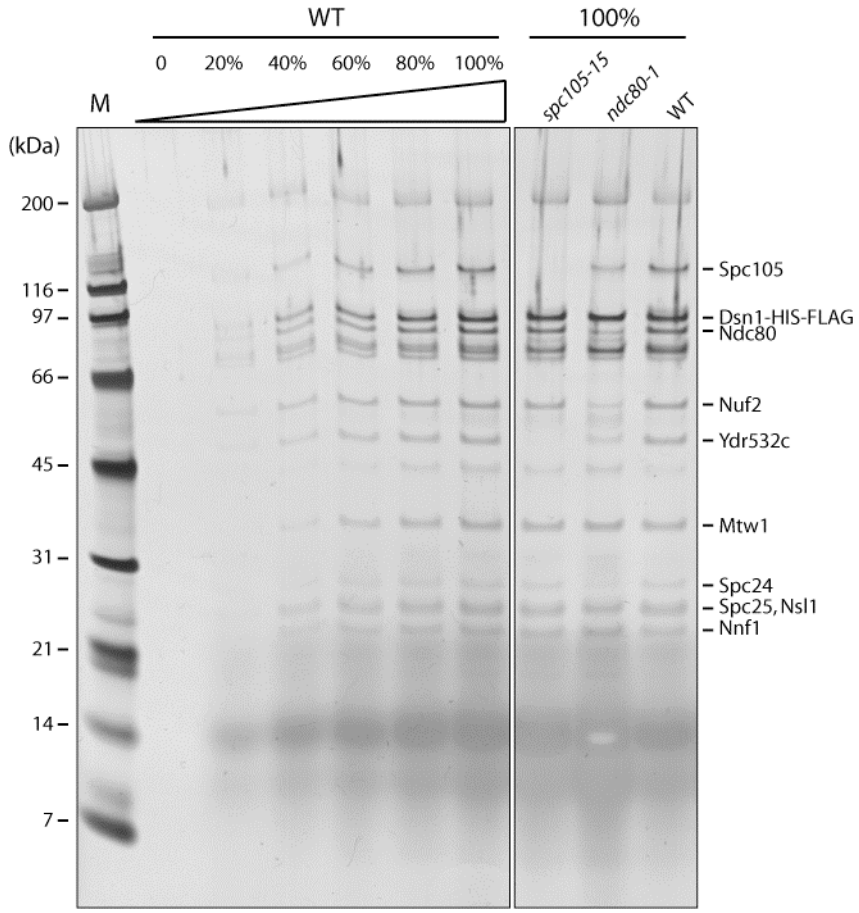

Figure S4. Composition of *ndc80-1* and *spc105-15* mutant kinetochore particles.

Kinetochore particles purified from WT, *ndc80-1,* and *spc105-15* cells were analyzed by SDS-PAGE followed by silver-staining. Serial dilutions of WT sample were loaded to determine the amount of specific kinetochore proteins in the mutant purifications relative to WT. We estimate that kinetochore material purified from *spc105-15* mutant cells contains ~80% of Ndc80 and Nuf2, and <20% of Spc105-15 and Ydr532c, relative to WT. The material from *ndc80-1* mutant cells appears to contain ~30% of Ndc80-1 and Nuf2, and ~45% of Spc105 and Ydr532c.

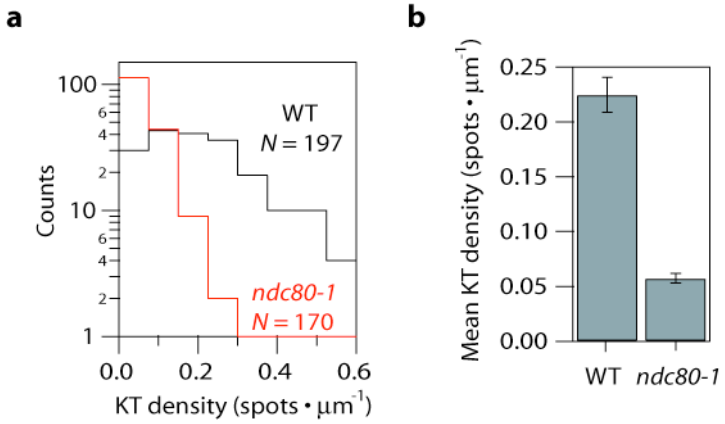

Figure S5. Ndc80-dependent binding of fluorescent kinetochore particles to taxol-stabilized microtubules.

Purified kinetochore particles from strains containing Cse4-GFP were incubated with fluorescent, taxol-stabilized microtubules at a concentration low enough to allow resolution of individual fluorescent particles (1 nM Dsn1-FLAG), as shown in Fig 2c. **a**, Distributions showing the number of Cse4-GFP kinetochore particles bound per unit-length microtubule for wild-type (WT, black) and *ndc80-1* (red) particles. **b**, On average, wild-type Cse4-GFP kinetochore particles exhibited ~4-fold greater binding than *ndc80-1* particles. Bars represent mean ± s.e.m., computed from the data in (**a**).

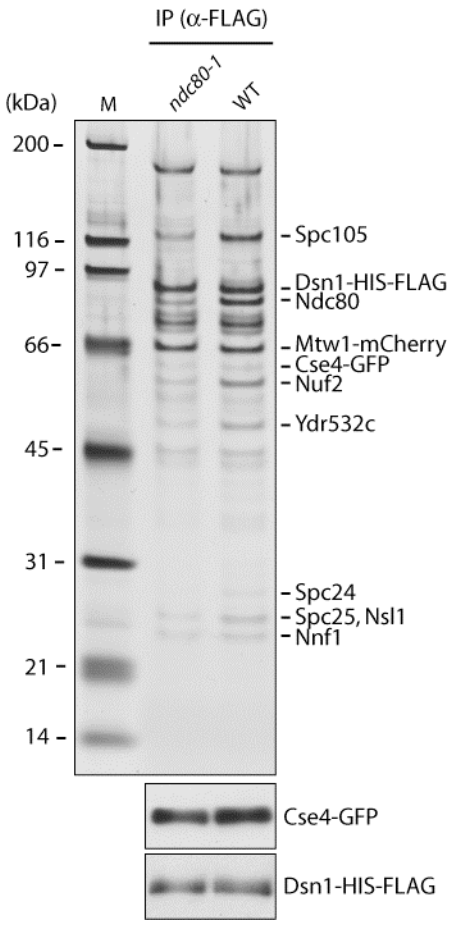

Figure S6. Cse4-GFP is present in the kinetochore particles purified from *ndc80-1* mutant cells.

Kinetochore particles were purified from *NDC80* (WT) or *ndc80-1* cells expressing Cse4-GFP. Purified samples were analyzed by SDS-PAGE followed by silver-staining (top) as well as by immunoblots against Cse4 and Dsn1-HIS-FLAG (bottom).

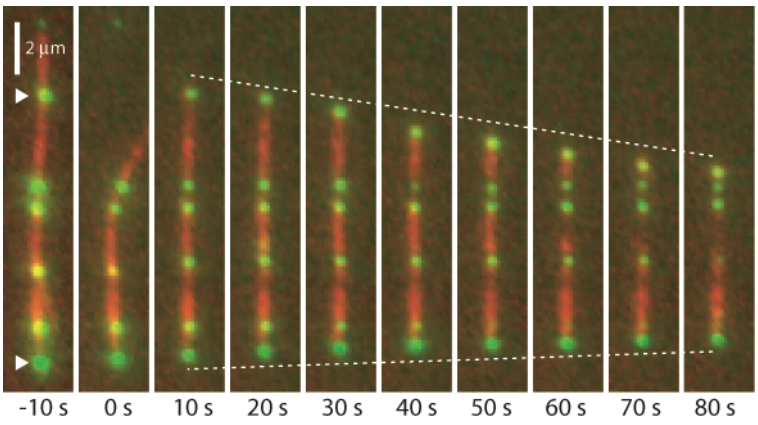

Figure S7. Disassembly-driven movement of Nuf2-3GFP kinetochore particles.

Selected frames from Movie S2 showing processive movement of Nuf2-3GFP kinetochore particles (green spots identified by arrowheads) on the ends of a shortening microtubule (red filament). Microtubules were polymerized from Alexa 647 tubulin in the presence of kinetochore particles (at 0.6 nM Dsn1-FLAG). Depolymerization was induced by rapid dilution of free tubulin at $t = 0$ seconds (dotted lines indicate period of disassembly).

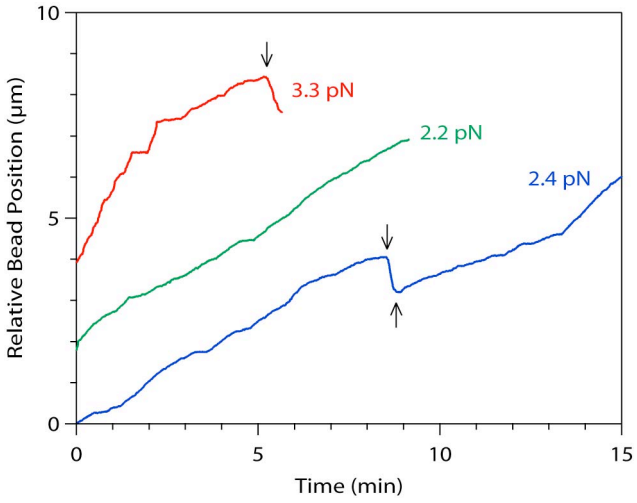

Figure S8. Additional example traces showing that kinetochore particles can couple tension to dynamic microtubules.

Records of position versus time for native kinetochore-based attachments subjected continuously to the indicated level of tensile force. Increasing position represents movement associated with microtubule assembly and decreasing position represents movement driven by disassembly. Arrows mark transitions in growth state (i.e., catastrophe and rescue). For clarity, traces are offset vertically by an arbitrary amount. These data were recorded using kinetochore particles after S-500 size exclusion chromatography (fraction #44, Figs. 1d and S3).

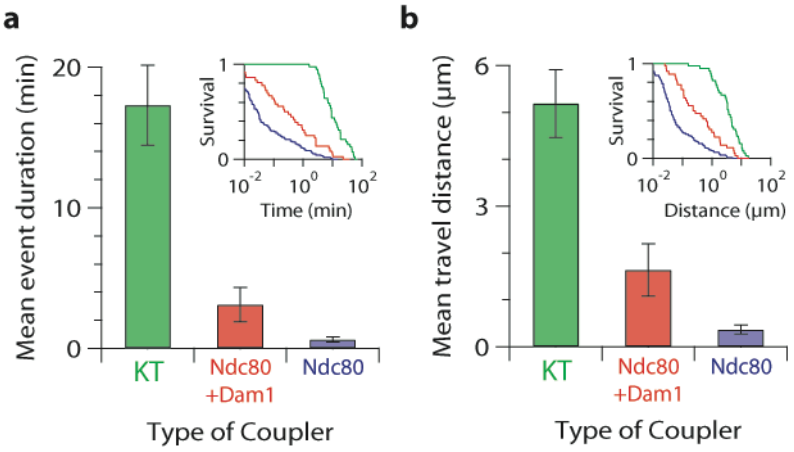

Figure S9. Coupling by kinetochore particles is more robust than simpler couplers based on recombinant Ndc80 and Dam1 subcomplexes.

a and **b**, Average event duration (**a**) and travel distance (**b**) for native kinetochore-based couplers, for couplers composed of bead-bound Ndc80 complexes alone, and for bead-bound Ndc80 in the presence of free Dam1 complex, undergoing assembly- and disassembly-coupled movement under tensile force. Bars represent mean ± s.e.m. Insets show survival probability for native kinetochore-based couplers (green trace), for couplers composed of bead-bound Ndc80 complex alone (blue trace), and for bead-bound Ndc80 in the presence of free Dam1 complex (red trace). $N = 40$, 37, and 112 events, respectively. Data for native kinetochore-based couplers were recorded at 1.9 ± 0.4 pN (mean ± s.d.), using beads prepared at a Dsn1:bead ratio of 200:1 (1.2 nM Dsn1-HIS-FLAG, 5.6 pM beads). Data for recombinant subcomplexes[3] were recorded at 1.8 ± 0.4 pN (mean ± s.d.), using beads with >2,000 Ndc80:bead (>13 nM Ndc80 complex, 6 pM beads), in the absence and presence of ~10 nM Dam1 complex.

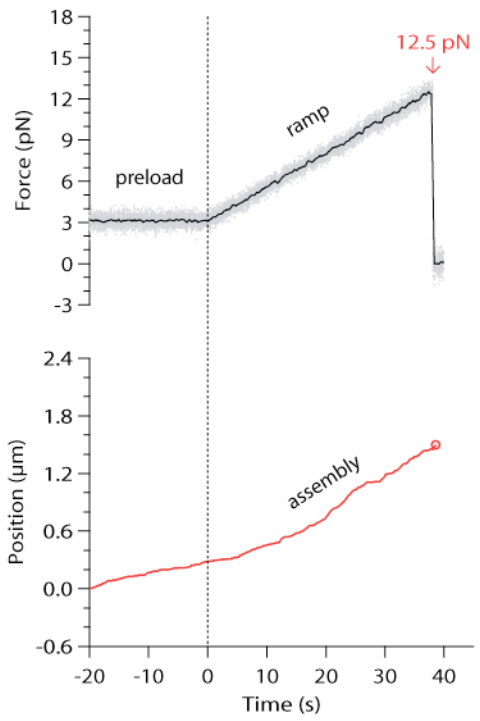

Figure S10. Measurement of rupture force for a bead-bound kinetochore particle attached to an assembling microtubule.

Representative record showing tensile force (upper plot) and position (lower plot) versus time for a bead associated with the assembling tip of a microtubule. The instrument was programmed to automatically ramp the force at a constant rate (0.25 pN s^{-1}) after a brief preload period (during which the force was held constant). Arrow marks maximum force, recorded when the attachment ruptured. Circle marks rupture on lower plot. For this particular event, the beads were prepared with kinetochore particles at a Dsn1:bead ratio of 200:1 (1.2 nM Dsn1-HIS-FLAG, 5.6 pM beads).

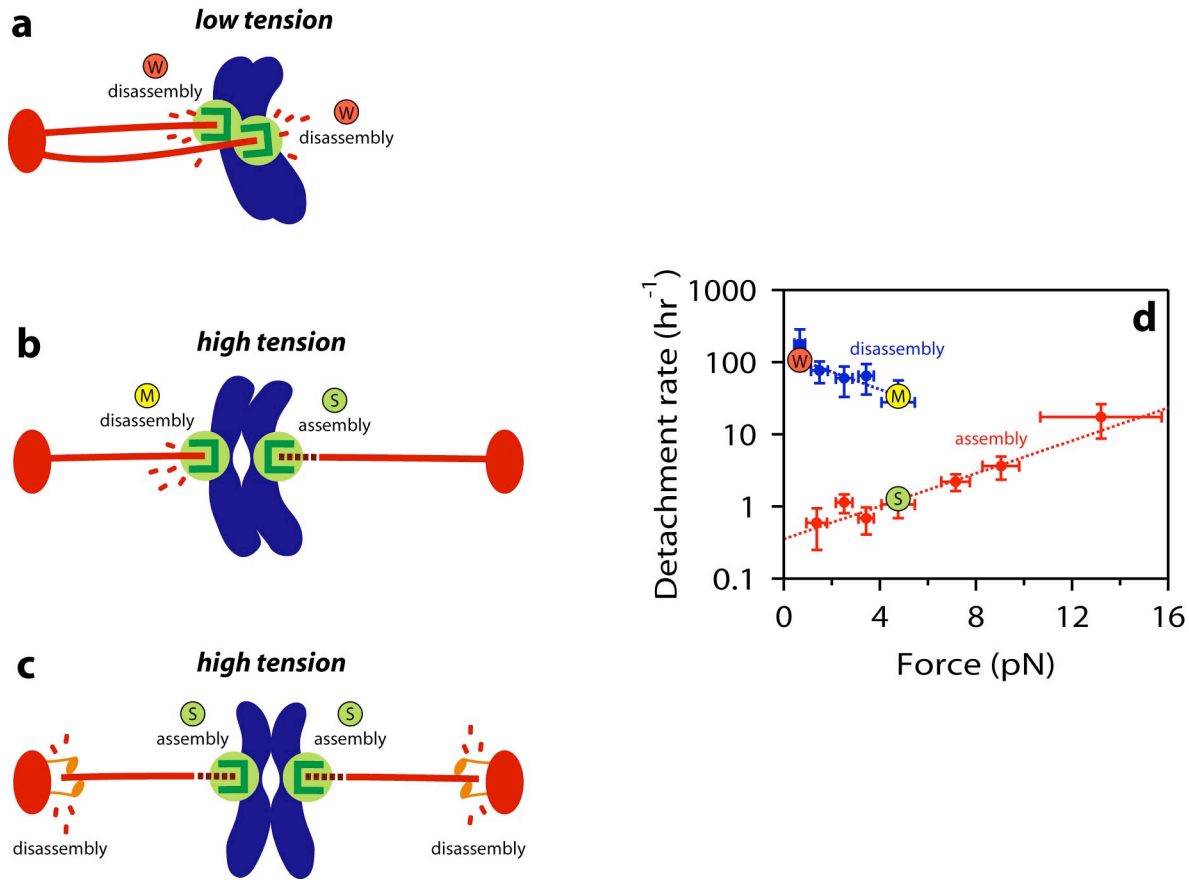

Figure S11. How tension-dependent modulation of tip dynamics could help selectively stabilize bi-oriented attachments *in vivo*.

a - c, For simplicity, we consider three scenarios where the sister kinetochores (large green circles) on a pair of sister chromatids (blue) are each attached to single microtubule tips (red filaments). Qualitatively similar behavior is expected for larger kinetochores that bind multiple tips. **a**, 'syntelic' case. Both sister kinetochores are attached to the tips of microtubules that emanate from the same spindle pole (large red ovals represent poles). Opposing spindle forces do not develop, so tension at both attachments is low. Both tips remain in the disassembling state and, consequently, both attachments are weak (marked here and in **d** by 'W' in small red circle). **b**, 'bi-oriented' case without poleward

flux. Sister kinetochores are attached correctly to the tips of microtubules emanating from opposite sides of the spindle, which generates high tension. The right tip is assembling, so the right attachment is strong ('S' in small green circle). The left tip is disassembling, so the left kinetochore is more vulnerable to detachment than its sister. However, relative to the kinetochores in **a**, it is moderately stabilized ('M' in yellow circle) because tension moderately inhibits detachment during disassembly (as shown in **d**, and in Fig. 4c). **c**, 'bi-oriented' case with poleward flux. Kinetochores attach tips from opposite sides, generating tension as in **b**. In this case, however, continuous poleward flux of the microtubules occurs, driven by traction forces (orange motors) and balanced by disassembly at the poles. Poleward flux allows simultaneous and persistent assembly of both kinetochore-attached tips, so both kinetochores are strongly attached. **d**, Data and fits from Fig. 4c with markers indicating hypothetical detachment rates for the kinetochores in **a** – **c** (assuming forces of ~0.5 and ~5 pN for syntelic and bi-oriented attachments, respectively). Given these detachment rates, the probability for scenario **a** to revert to a singly-attached ('monotelic') state would be 6-fold higher than scenario **b**, and 100-fold higher than scenario **c**. Thus, in either scenario selective stabilization of bi-oriented attachments would occur.

2. Supplementary Notes

Note S1. Spectral counts normalized to protein length[4] indicate that the KMN subcomplexes are the most abundant in the sample and the other core kinetochore proteins are present at relatively lower stoichiometry (Table S1), consistent with the silver-staining results (Fig. S2), and with fluorescence microscopy studies suggesting that the yeast KMN and Dam1 subcomplexes are most abundant on bi-oriented kinetochores[5]. Although the levels of Dam1 in our purifications are lower than KMN, kinetochores that are not attached to microtubules *in vivo* also have lower levels[6,7].

Note S2. Most of the CBF3 complex was not detected by mass spectrometry, consistent with the possibility that DNA may not co-purify with Dsn1-FLAG.

Note S3. We concentrated the peak fraction (#44) after gel filtration and found that the pattern on a silver-stained SDS-PAGE gel was similar to the FLAG eluate (data not shown), suggesting that the relative stoichiometry of core kinetochore proteins is similar before and after gel filtration.

Note S4. Our data provide strong evidence that the kinetochore particles must interact with the tips of the microtubules, because particle movement is driven by disassembling tips (Figs. 2 and 3) and because tension applied through the particles affects the dynamics of both growing and shortening tips (Fig. 4). However, the geometric arrangement of the kinetochore particles relative to the microtubule ends is uncertain. In principle, the particles could interact primarily with the 'outer' faces of the α/β tubulin dimers, which

are exposed in the lattice and also near the tip. Additionally, they could interact with structures that are found only at tips (i.e., exposed 'longitudinal', 'lateral', or 'lumenal' faces of the tubulin, or curved tubulin oligomers[8]). Also, the particles may or may not make 'end-on' attachments that resemble structurally those seen by electron microscopy in metazoans, where the kinetochores appear as a roughly planar fibrous meshwork and the microtubule tips are embedded nearly perpendicularly in the mesh[9].

Note S5. We found no evidence that the particles can track with growing tips in the absence of externally applied tension, i.e. 'autonomously'. However, we note that tip-attached kinetochores *in vivo* are usually under tension[10], and they are not known to track autonomously with growing tips. Instead, when the tension on a tip-attached kinetochore that is moving anti-poleward is suddenly lost (e.g., by laser ablation of its sister), the kinetochore ceases to move and adopts a 'neutral' or paused state[11]. This is similar to the behavior of the kinetochore particles: if a kinetochore-decorated bead is at first pulled so that it associates persistently with a growing microtubule end, and then the force is suddenly removed (by shuttering the laser trap), the bead ceases to move with the growing end. Likewise, fluorescent particles that appear initially to be bound at or near growing ends do not track with growth.

Note S6. Kinetochores in budding yeast are each thought to contain about six copies of Dsn1 (based on quantitative fluorescence measurements *in vivo*[5] and on the stoichiometry of proteins comprising the Mis12 subcomplex[1]). If the purified kinetochore particles also contain six Dsn1 molecules, then a Dsn1:bead ratio of 200:1 corresponds to a maximum

of ~33 particles per bead. Simple geometric considerations indicate that particles on only a small fraction of the bead surface, < 7 %, could simultaneously interact with a microtubule[12], indicating that coupling at low Dsn1:bead ratios was probably due to single kinetochore particles (see also, Fig. 3).

Note S7. The mean lifetime of attachment is equivalent to the mean first-passage time for detachment, $\langle t \rangle$, which can be expressed as a function of individual rate constants for any kinetic scheme with a finite number of states[13]. For the two-state catch bond-like model with the kinetochore initially bound to an assembling tip, the mean first-passage time is given by,

$$\langle t \rangle = \frac{k_1 + k_2 + k_4}{k_1 k_4 + k_2 k_3 + k_3 k_4},$$

where k_1, k_2, k_3, and k_4, represent the rates of catastrophe, rescue, detachment from assembly, and detachment from disassembly, respectively (the same rates displayed in Fig. 4b, 4c and 4d). The predicted lifetime curve in Fig. 4a was computed by substituting the best-fit exponential functions (Table S2) into the equation above.

3. Supplementary Tables

Table S1. Dsn1-FLAG MS list (excel file link).

Table S2. Parameters for exponential curve fits shown in Fig. 4c and 4d. The force dependence of all four rates, k_1, k_2, k_3, k_4, was fit with the equation, $k_n(F) = k_n^o \, exp\{F/F_n\}$, where F represents the applied force. The constants k_n^o and F_n represent the unloaded rate and the force required for an *e*-fold change, respectively.

n	**Transition**	**Unloaded rate** k_n^o (hr^{-1})	**Sensitivity** F_n (pN)
1	catastrophe	6.7 ± 2.0	-2.3 ± 0.5
2	rescue	86 ± 28	6.4 ± 4.2
3	detachment during assembly	0.4 ± 0.1	3.8 ± 0.8
4	detachment during disassembly	125 ± 61	-4.0 ± 3.1

Table S3. Yeast strains used in this study. All strains are isogenic with the W303 background.

Strain	Genotype	Used in Figure
SBY3	*MAT**a** ura3-1 leu2,3-112 his3-11 trp1-1 ade2-1 LYS2 can1-100 bar1Δ*	1a, b, S1, S2
SBY5640	*MAT**a** ura3-1::CSE4-3FLAG::URA3 leu2,3-112 his3-11 trp1-1::256lacO:TRP1 ade2-1 LYS2 can1-100 cse4Δ::KAN PDS1-18myc::LEU2*	S1
SBY7441	*MAT**a** ura3-1 leu2,3-112 his3-11 trp1-1 ade2-1 lys2 can1-100 bar1Δ DSN1-3FLAG::KAN*	1a, b, c, S1, S2
SBY7464	*MAT**a** ura3-1 leu2,3-112 his3-11 trp1-1 ade2-1 lys2 can1-100 bar1Δ DSN1-3FLAG::KAN NDC80-13myc::KAN*	S2
SBY7492	*MAT**a** ura3-1 leu2,3-112 his3-11 trp1-1 ade2-1 LYS2 can1-100 bar1Δ SPC105-3FLAG::TRP1*	S1
SBY7870	*MAT**a** ura3-1 leu2,3-112 his3-11 trp1-1 ade2-1 LYS2 can1-100 bar1Δ NUF2-3FLAG::KAN*	S1
SBY8193	*MAT**a** ura3-1 leu2,3-112 his3-11 trp1-1 ade2-1 lys2 can1-100 bar1Δ DSN1-3FLAG::KAN NUF2-3GFP::HIS3*	S2, S7
SBY8253	*MAT**a** ura3-1 leu2,3-112 his3-11 trp1-1 ade2-1 can1-100 LYS2 bar1Δ DSN1-6HIS-3FLAG::URA3*	1d, 2a, 3, 4, S1, S2, S3, S4, S8, S9, S10
SBY8332	*MAT**a** ura3-1 leu2,3-112 his3-11 trp1-1 ade2-1 can1-100 LYS2 bar1Δ DSN1-6HIS-3FLAG::URA3 NUF2-3GFP::HIS3 MTW1-mCherry::HPH*	S2
SBY8334	*MAT**a** ura3-1 leu2,3-112 his3-11 trp1-1 ade2-1 can1-100 LYS2 bar1Δ DSN1-6HIS-3FLAG::URA3 NUF2-3GFP::HIS3 MIF2-mCherry::HPH*	S2
SBY8362	*MAT**a** ura3-1 leu2,3-112 his3-11 trp1-1 ade2-1 can1-100 LYS2 bar1Δ DSN1-6HIS-3FLAG::URA3 ndc80-1*	2a, 3, S4
SBY8381	*MAT**a** ura3-1 leu2,3-112 his3-11 trp1-1 ade2-1 can1-100 LYS2*	2a, 3, S4

	bar1Δ DSN1-6HIS-3FLAG::URA3 spc105-15	
SBY8460	*MAT**a** ura3-1 leu2,3-112 his3-11 trp1-1::256lacO::TRP1 ade2-1 can1-100 LYS2 bar1Δ DSN1-6HIS-3FLAG:URA3 dad1-1::KAN*	2a, 3
SBY8505	*MAT**a** ura3-1 leu2,3-112 his3-11 trp1-1 ade2-1 can1-100 LYS2 bar1Δ DSN1-6HIS-3FLAG::URA3 YDR532c-GFP::HIS3*	S2
SBY8506	*MAT**a** ura3-1 leu2,3-112 his3-11 trp1-1 ade2-1 can1-100 LYS2 bar1Δ DSN1-6HIS-3FLAG::URA3 SPC105-GFP::HIS3*	S2
SBY8564	*MAT**a** ura3-1 leu2,3-112 his3-11 trp1-1 ade2-1 LYS2 can1-100 bar1Δ MTW1-3FLAG::KAN*	S1
SBY8584	*MAT**a** ura3-1::CSE4-GFP::URA3 leu2,3-112 his3-11 trp1-1 ade2-1 can1-100 lys2 bar1Δ DSN1-6HIS-3FLAG::URA3 cse4Δ::KAN*	S2
SBY8678	*MAT**a** ura3-1::CSE4-GFP::URA3 leu2,3-112 his3-11 trp1-1 ade2-1 can1-100 lys2 bar1Δ DSN1-6HIS-3FLAG::URA3 cse4Δ::KAN MTW1-mCherry::HPH ndc80-1*	2c, S5, S6
SBY8680	*MAT**a** ura3-1::CSE4-GFP::URA3 leu2,3-112 his3-11 trp1-1 ade2-1 can1-100 lys2 bar1Δ DSN1-6HIS-3FLAG::URA3 cse4Δ::KAN MTW1-mCherry::HPH*	2c, 2d, S5, S6

Table S4. Plasmids used in this study.

Plasmid	Description
pBS35	*mCherry, HPH* (gift from Yeast Resource Center (mCherry from Roger Tsien)
pGEX-2T	*GST expression vector*
pSB167	*12Myc, URA3* (integrating)
pSB450	*pFA6a-TRP1*
pSB623	*3GFP, HIS3* (gift from David Pellman, PB1585)
pSB624	*DSN1, CEN, URA3*
pSB812	*3FLAG, KAN* (gift from Toshi Tsukiyama, p3FLAG-KANMX)
pSB897	*NUF2-3GFP, HIS3* (integrating)
pSB1110	*DSN1-12Myc, URA3* (integrating)
pSB1113	*DSN1-3FLAG, URA3* (integrating)
pSB1265	*3FLAG, TRP1*
pSB1590	*DSN1-6HIS-3FLAG, URA3* (integrating)
pSB1617	*CSE4-GFP, URA3* (integrating)
pSB1643	*GST-SPC105 (1-798 bp) expression vector*

4. Supplementary Movie legends

Movie S1. Cse4-GFP kinetochore particles track with depolymerizing microtubule tips.

Dynamic microtubules were polymerized from Alexa 647 tubulin in the presence of Cse4-GFP kinetochore particles (at 10 nM Dsn1-FLAG). Depolymerization was triggered by removing the free tubulin via buffer exchange, causing a significant decrease in red background fluorescence and subsequent disassembly-driven movement of microtubule-bound kinetochore particles (arrows indicate the filament shown in Fig. 2d). The movie was recorded at 10 frames s^{-1} and is displayed here at ×10 speed. Scale bar, 3 μm.

Movie S2. Nuf2-3GFP kinetochore particles track with shortening tips.

This movie (corresponding to the microtubule shown in Fig. S7) was collected using the same protocol as Movie S1, with the exception that kinetochore particles were labeled via Nuf2-3GFP. It was recorded at 10 frames s^{-1} and is displayed here at ×4 speed. Scale bar, 2 μm.

Movie S3. Purified kinetochore particles couple force to dynamic microtubules.

Movement of an end-associated bead is coupled to multiple rounds of microtubule assembly and disassembly under 1.7 pN of constant tension, applied by a laser trapping-based force clamp. The end-associated bead is held in a fixed position in the laser trap while the stage is moved under feedback control to accommodate changes in microtubule length. A second bead, stuck to the coverslip, serves as a fiducial illustrating the stage

movement. Leftward movement corresponds to filament growth and rightward movement corresponds to shortening. Beads were prepared with kinetochore material at a Dsn1:bead ratio of 200:1. The movie was recorded at 30 frames s^{-1} using differential interference contrast microscopy and is shown here at ×60 speed.

5. Supplementary References

1. De Wulf, P., McAinsh, A. D. & Sorger, P. K. Hierarchical assembly of the budding yeast kinetochore from multiple subcomplexes. *Genes Dev* **17**, 2902-2921 (2003).

2. Wei, R. R., Sorger, P. K. & Harrison, S. C. Molecular organization of the Ndc80 complex, an essential kinetochore component. *Proc Natl Acad Sci U S A* **102**, 5363-5367 (2005).

3. Tien, J. F. *et al.* Cooperation of the Dam1 and Ndc80 kinetochore complexes enhances microtubule coupling and is regulated by aurora B. *J Cell Biol* **189**, 713-723 (2010).

4. Liu, H., Sadygov, R. G. & Yates, J. R., 3rd. A model for random sampling and estimation of relative protein abundance in shotgun proteomics. *Anal Chem* **76**, 4193-4201 (2004).

5. Joglekar, A. P., Bouck, D. C., Molk, J. N., Bloom, K. S. & Salmon, E. D. Molecular architecture of a kinetochore-microtubule attachment site. *Nat Cell Biol* **8**, 581-585 (2006).

6. Li, Y. *et al.* The mitotic spindle is required for loading of the DASH complex onto the kinetochore. *Genes Dev* **16**, 183-197. (2002).

7. Enquist-Newman, M. *et al.* Dad1p, third component of the Duo1p/Dam1p complex involved in kinetochore function and mitotic spindle integrity. *Mol Biol Cell* **12**, 2601-2613. (2001).

8. McIntosh, J. R. *et al.* Fibrils connect microtubule tips with kinetochores: a mechanism to couple tubulin dynamics to chromosome motion. *Cell* **135**, 322-333 (2008).

9. McEwen, B. F. & Dong, Y. Contrasting models for kinetochore microtubule attachment in mammalian cells. *Cell Mol Life Sci* **67**, 2163-2172 (2010).

10. Waters, J. C., Skibbens, R. V. & Salmon, E. D. Oscillating mitotic newt lung cell kinetochores are, on average, under tension and rarely push. *J Cell Sci* **109**, 2823-2831 (1996).

11. Khodjakov, A. & Rieder, C. L. Kinetochores moving away from their associated pole do not exert a significant pushing force on the chromosome. *J Cell Biol* **135**, 315-327 (1996).

12. Powers, A. F. *et al.* The Ndc80 kinetochore complex forms load-bearing attachments to dynamic microtubule tips via biased diffusion. *Cell* **136**, 865-875 (2009).

13. Shaevitz, J. W., Block, S. M. & Schnitzer, M. J. Statistical kinetics of macromolecular dynamics. *Biophys J* **89**, 2277-2285 (2005).